Terr. Atmos. Ocean. Sci., Vol. 21, No. 5, 767-779, October 2010 doi: 10.3319/TAO.2009.10.27.01(T)

Significance of Prehistoric Liquefaction Features in the Xilinhot District, Inner Mongolia, Northern China

Jianguo Du[1, *], Bihong Fu[2], Wensheng Guo[3], Lin Du[4], Jiayi Zou[3], Xiaocheng Zhou[1], and Li Yi[1]

[1] *Institute of Earthquake Science, China Earthquake Administration, Beijing 100036, China*
[2] *Institute of Geology and Geophysics, Chinese Academy of Sciences, Beijing 100029, China*
[3] *Inner Mongolian Bureau of Seismology, Hohhot 010051, China*
[4] *Faculty of Engineering, Building, Civil, and Environmental Engineering, Concordia University, Montreal, Quebec H3G 1M8, Canada*

Received 25 August 2009, accepted 27 October 2009

ABSTRACT

Paleo-ground ruptures, fissures, liquefaction and geomorphic features in the Xilinhot district, Inner Mongolia, northern China, are documented and seismic intensity for the meizoseismal areas and magnitudes of paleoearthquakes are estimated. Trenching investigations revealed a huge paleoseismic ground rupture and fissure zone with a width of more than 200 m. Field investigations and interpretation of remote sensing images demonstrate that active faults related to paleoearthquakes appear to be about 200 km long. Geologic and geomorphic evidences indicate that one large earthquake with a magnitude of about 7.5 at about 13 ka BP or multiple paleoseismic events of $M \geq 6.0$ have occurred in the studied area since 53 ka BP. One of the paleo-meizoseismal areas is determined to be near Xilinhot. Seismic intensity in Modified Mercalli scale (MM) is estimated to be larger than VI in the vicinity of the study area and at least VIII in the epicentral region. This is consistent with seismic activities in and around the Xilinhot district in recent years, but higher than anything yet reported. The results provide important data for design engineering and regional planning in order to resist damage from potentially large earthquakes in the future.

Key words: Seismic intensity, Liquefaction, Rupture, Active fault, Paleoearthquake, Inner Mongolia

Citation: Du, J., B. Fu, W. Guo, L. Du, J. Zou, X. Zhou, and L. Yi, 2010: Significance of prehistoric liquefaction features in the Xilinhot district, Inner Mongolia, northern China. Terr. Atmos. Ocean. Sci., 21, 767-779, doi: 10.3319/TAO.2009.10.27.01(T)

1. INTRODUCTION

Since 2000, several disastrous earthquakes have occurred in continental regions where active faults that have displaced since 100 ka BP had not been previously mapped in detail (Fu et al. 2004; González de Vallejo et al. 2005). For example, the M_w 6.6 Bam earthquake struck southeastern Iran on 26 December 2003, which killed over 43000 people, injured 20000, left 60000 homeless, and destroyed most of the city of Bam (Fu et al. 2004). The 12 May 2008 M_s 8.0 Wenchuan earthquake occurred in the region where seismic intensity was estimated to be VII (MM), but approached XI in the epicentral area, and left about 100 thousand persons dead. Likewise, the Xilinhot district, Inner Mongolia, lacks a seismic network and was considered to have very low seismicity. However, recent seismic activity and the new found liquefaction in the Xilinhot district indicate that the seismic intensity of this area needs to be reevaluated. Therefore, it is necessary to investigate active faults and seismic activities in order to mitigate earthquake hazard in the region.

Geologic and geomorphic features related to seismic faults are widely used to determine the location, size, and frequency of strong paleoearthquakes and to understand both short-term and long-term seismic hazards (McCalpin 1996; Obermeier 1996; Yeats et al. 1997; Prestininzi and Romeo 2000; Huang et al. 2008). Additionally, for studying earthquake-induced/seismogenic active faults and seismic hazards, high-resolution satellite remote sensing techniques are very useful, especially in arid regions (Peltzer et al. 1999; Fu et al. 2003). Liquefaction, sand blow, sand dikes and fissures resulted from ground shaking are very commonly related to seismic activity and are classified as secondary features of large earthquakes (McCalpin 1996; Yeats et al. 1997). Therefore, active faults, paleo-ground

* *Corresponding author*
E-mail: jianguodu@hotmail.com

ruptures, fissures and liquefaction features are important geological records of paleoearthquakes, which can extend our knowledge of seismic activity into the prehistoric period (McCalpin 1996; Yeats et al. 1997; Ran and Deng 1999; Tuttle 2001). Prehistoric seismic events can be studied by investigating surface-rupturing history, identifying seismic liquefaction effects, and trenching active faults (Obermeier 1998; Vanneste et al. 2001; Olson et al. 2005). Obermeier (1998) and Obermeier and Pond (1999) addressed many current technical issues in using liquefaction features for paleoseismic analysis. For estimating quantitatively the peak ground acceleration and paleoearthquake magnitude based on liquefaction features, Olson et al. (2005) briefly evaluated the most widely used techniques, the cyclic stress method (Green 2001) and the magnitude-bound method (e.g., Ambraseys 1988), and proposed a new approach. Green et al. (2005) discussed the techniques for estimating ground surface acceleration and paleoearthquake magnitude, and for verifying the estimated provisional location of the energy center of paleoearthquakes.

Very few active fault investigations have been conducted in the Xilinhot district, Inner Mongolia Autonomous Region, because the region is located in a remote area of northern China (Fig. 1). This is why the Xilinhot district was considered to be lacking in strong earthquakes and active faults (Ding 1991). The seismic intensity in the Xilinhot district was estimated to be less than VI (MM) on the seismic zoning map of China in 1990 (CSB 1991), and the value of peak ground acceleration was less than 0.01 m s^{-2} on the zoning map of ground vibration parameters in China in 2001 (CSB 2001). Engineering geology investigations have been conducted in recent years in order to evaluate the suitability of locations for several planned power plants in the Xilinhot district. This paper aims at reporting new findings related to paleoearthquakes and seismic faults in the area and presents the current understanding of seismic activity and intensity in the Xilinhot district.

2. SEISMOGEOLOGICAL SETTING

The Xilinhot district is located along the southeastern tectonic boundary of the Bayinhesuo basin which is part of the NE-SW-trending tectonic zone of Daxinganlin Mountain (Ding 1991). The active faults can be classified into three groups: the first one extends NE-SW, the second with a strike of NW-SE, and the third striking near E-W. These faults have been designated as Early Pleistocene in age, and only one fault, oriented NE, crosses the southeast part of the study area (Fig. 1). Active faults, which activated after the beginning of Holocene (11.5 ka; Ding 1991; Ran and Deng 1999), have not been thoroughly described in the Xilinhot district. There are many Early Pleistocene craters and plenty of basalts that were derived from the upper mantle in the Xilinhot district (BGMRIM 1991) and formed the flat tops of many hills. This indicates that faults penetrate the crust and an abundance of heat derived from the mantle could

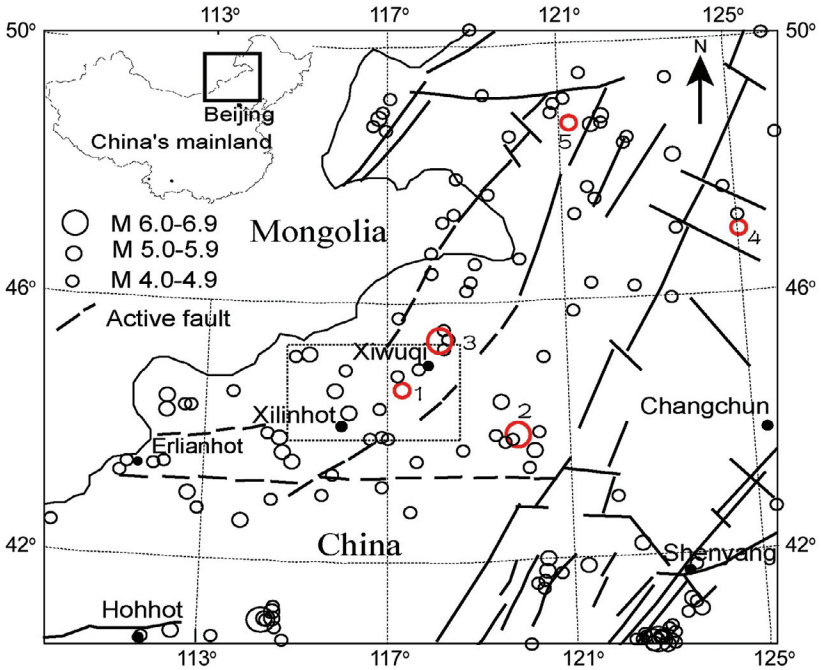

Fig. 1. Active faults and seismic activity in the study area and vicinity. Active faults (modified after Ding 1991) and epicenter distribution of $M_L \geq 4.0$ earthquakes in the Xilinhot district (the insert square corresponding to Fig. 2) and vicinity from January 1970 to April 2005 (data from the Data Base of CEA), the insert showing the location of the study area (dashed square), and red thick circles No. 1 to 5 are earthquakes occurred in 20 October 2002 (M_s 4.7), 16 August 2003 (M_s 5.7), 24 March 2004 (M_s 6.0), 25 July 2005 (M_s 5.2) and 3 May 2006 (M_s 4.2), respectively.

have been carried to the crust and up to the surface. Distributions of epicenters of $M_L \geq 4.0$ earthquakes from January 1970 to April 2005 in the Xilinhot district and vicinity indicate that historically, strong earthquakes rarely occurred before 2001. However, several strong earthquakes have occurred in the region in the past years (Fig. 1). Our field investigations indicated that no ground ruptures occurred after these strong earthquakes, but a few small fissures were found in the epicenter areas.

Quaternary slack sediments are distributed in the intermountain basins such as the Bayinhesuo basin. Mesozoic indurated continental deposits and igneous rocks are exposed on mountains and hills in the study area and vicinity. Quaternary sediments in the profiles consist of three layers; the lower layer belongs to the Middle to Lower Pleistocene Series (Q_{1-2}), the middle layer to the Later Pleistocene (Q_3), and the upper layer to Holocene (Q_4) soil. The Middle Pleistocene Series (Q_2) are absent in the study area (BGMRIM 1991). The Quaternary sediments contain the thick laminated sands with about 5% silt and clay, revealed in the four profiles of P1, P2, P3 and P4 in Fig. 2, providing proper materials for liquefaction (Fig. 3). Correlation of Quaternary sediments is briefly described as follow.

In Fig. 3, strata from the top to the bottom of profile No. 1 (P1), revealed by trenching, are: (a) 15 to 20 cm thick brown sandy soil; (b) thick laminated grey coarse sands; (c) laminated gray gravel interbedded with coarse sand, with a maximum thickness of 110 cm, pinching out gradually from SW to NE; and (d) the bottom layer of buff coarse sand showing small folds and disturbed structure, which is unconformable with the laminated gravel layer (c).

Profile No. 2 (P2), located about 11 km northeast of P1, contains mainly coarse sands: (a') about 10-cm thick brown soil of Holocene; (b') thick yellow coarse sands; (c') laminated coarse pelitic sand; and (d') thick gray coarse sand (Q_3).

Profile No. 3 (P3), located about 50 km southwest of P1, contains three layers from the top to bottom: (1) 20-cm thick Holocene-age soil, unconformable with (2); (2) 30-cm laminated coarse sands embedded with medium-grained sands; (3) 100-cm thick laminated medium-grained sands embedded with fine-grained sands; and (4) gray coarse sands with a disturbed structure.

At profile No. 4 (P4), located some 150 km northeast of P1, the strata from top to bottom of the section are: (A) 15-cm brown soil of Holocene age; (B) 40 cm thick light-brown pelitic and silty medium to coarse grained sands with disturbed structure; (C) 60-cm thick grayish-yellow coarse sands, the upper boundary was strongly deformed by liquefaction; and (D) > 150 cm thick yellow medium to coarse grained sands without clear lamination.

3. EVIDENCE FOR LARGE PALEOEARTHQUAKES

3.1 Geomorphic Features of Active Faults

Landsat Enhanced Thematic Mapper (ETM) and Digital Elevation Models (DEMs) from the Shuttle Radar Topography Mission (SRTM) were employed to identify geomorphic features related to active faults in this study. Spatial resolutions for Landsat ETM and SRTM's DEM data are 15 - 30 and 90 m, respectively. The remote sensing data were processed using ER-Mapper software. Two large

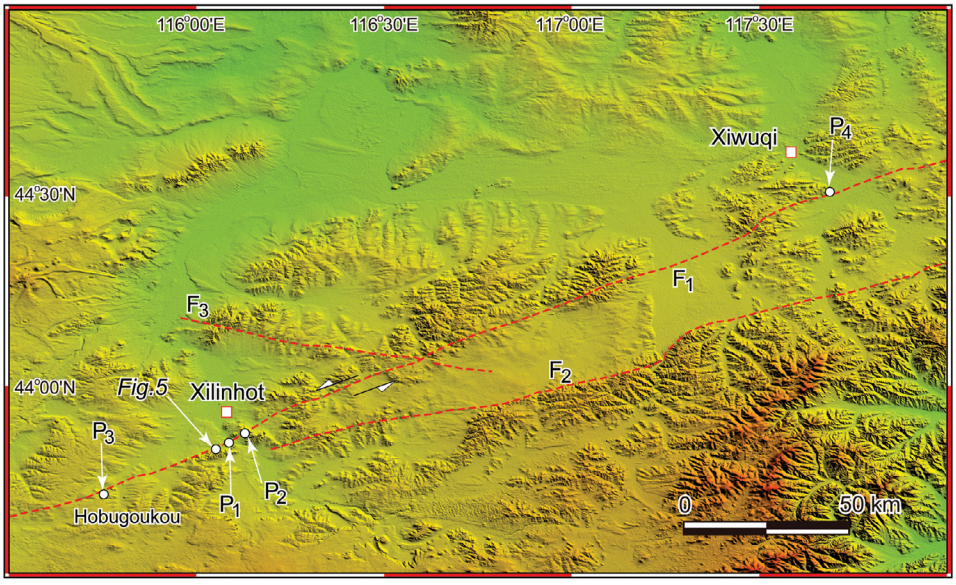

Fig. 2. Image generated from the SRTM DEM data showing the geomorphic features of the active faults, corresponding to the insert square area in Fig. 1, the red dashed lines show the active faults (F1, F3 and F3). The coordinates of the sites of P1, P2, P3 and P4 are 43°49'48.8''N, 116°05'09.82''E; 43°50'33.5''N, 116°07'37.5''E; 43°37'23.9''N, 115°39'38.8''E; and 44°31'28.9''N, 117°41'14.8''E, respectively.

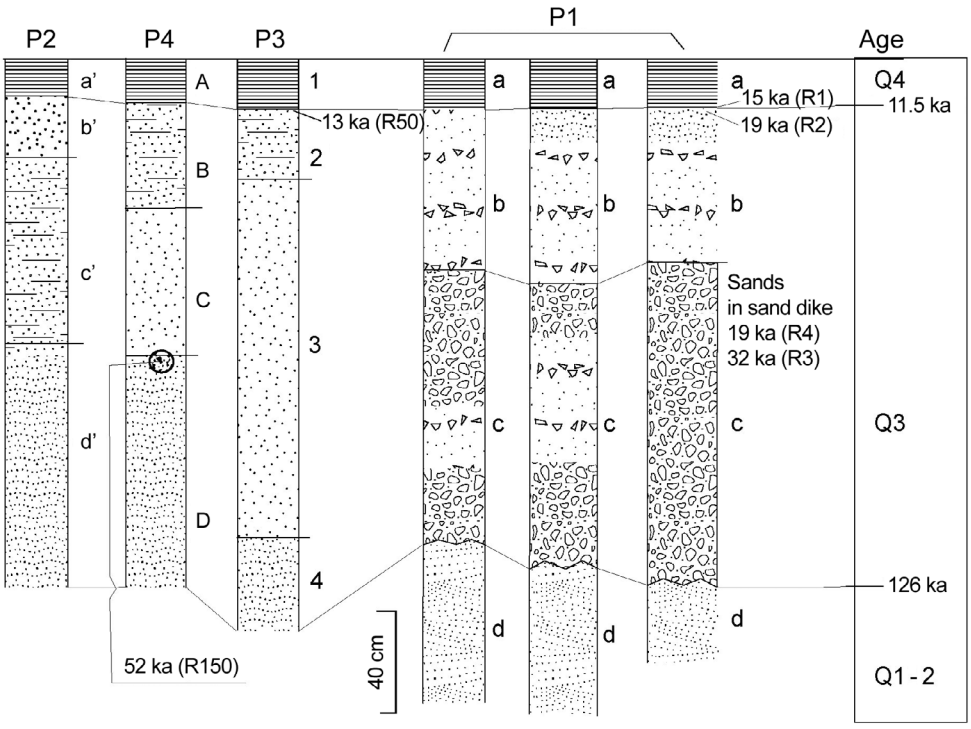

Fig. 3. Correlation of Quaternary strata, detailed stratigraphic description in the text.

NE-SW trend faults (F1 and F2) and one NW-SE fault (F3) were recognized from the satellite remote sensing image in which clear linear features of faults are displayed (Fig. 2). For verifying the faults, field investigations for F1 and F2 were conducted, and lateral offset of streams, paleo-ground ruptures and paleo-surface fissures are described here.

Xilinhot reservoir on the Xinlinhot River appears as a "Z" shape which can be ascribed to erosion along zone F1 as well as faulting displacement (Fig. 2). Some small streams 1 - 2 km to the southwest of site P1 were displaced, and the individual offsets range from 2 to 5 m (Fig. 4). At site P2, the occurrence of Quaternary sands on the two sides of a small valley oriented NE-SW is different. The sands have a dip direction of 180° and dip angle of 20° on the SE side, but a dip direction of 160° and dip angle of 15° on the NW side, indicating that the fault (F1) passes through the small valley, although no vertical dislocation of sand layer was evident there. Other strong evidence of displacement, such as a fault scarp or large stratum dislocation, was not observed in the field due to geomorphic changes, Holocene sediment covering, and lack of trenching.

3.2 Paleo-Ground Ruptures and Fissures

About 30 paleo-ground ruptures and paleo-surface fissures were observed along a 185-m long trench (P1) about 1.5 to 2 m deep with a surface dip of 10°NE (Fig. 5). Different paleo-liquefaction features observed at P1 are illustrated by Figs. 6 to 9. The paleo-surface is demonstrated by the unconformity between the soil layer and the underlying sands. The bottom of the soil developed in the sand-blow with a maximum thermoluminescence age of 15.2 ± 1.3 ka (Fig. 6, Table 1: R1) which is about 3.7 ka older than the beginning of the Holocene (11.5 ka). Beneath the sandy soil, sand dikes, sand blows, filled clast, intruded sands, and deformed sediment layers were encountered. Sand dikes commonly root in the depth range from 150 to 230 cm. The widths of dikes and sand-filled paleo-ground ruptures/fissures range from several centimeters to 120 cm, and the wider fissures can be attributed to surface waves and surface oscillation. Dike sands were transported upward, displayed on the vertical section, and some dikes have top terminations similar to the features of hydraulic fractures described by Obermeier (1996), indicating hydraulic fracturing. The sand-filled fissures with nominally constant width with depth (Figs. 6 - 9) were almost certainly caused by surface oscillations. The vertical displacement on the profile is slight. However, the upper part of the profile is severely folded (Figs. 7, 8). On detailed field observation, some sand dikes marked in Fig. 5 display structures that were formed by upward liquefied sand flow (e.g., Figs. 6 to 9). Paleo-ground ruptures and fissures with different strikes in P1, mainly 45, 10, and 80°NE, were found on both sides of the railway. Therefore, the zone of paleo-ground rupture and fissures is NE-SW trending. The fold and fissures, combined with linear distribution of evident displacement of river and streams, imply that the ac-

tive faults (Fig. 2) are related to large paleo-earthquakes.

At P3 (Hobugoukou), there is a ditch of approximately 15-cm-deep and more than 300 m formed long on the top of a ground fissure. The ground fissure with a strike of 40°NE at the NW part of P3 is 20 cm wide at 50 cm and 2 cm wide at 120 cm under the surface, and pinches out at a depth of 150 cm. The sand dike overlain by surface soil appears gravitationally deposited in liquid because of winnowing

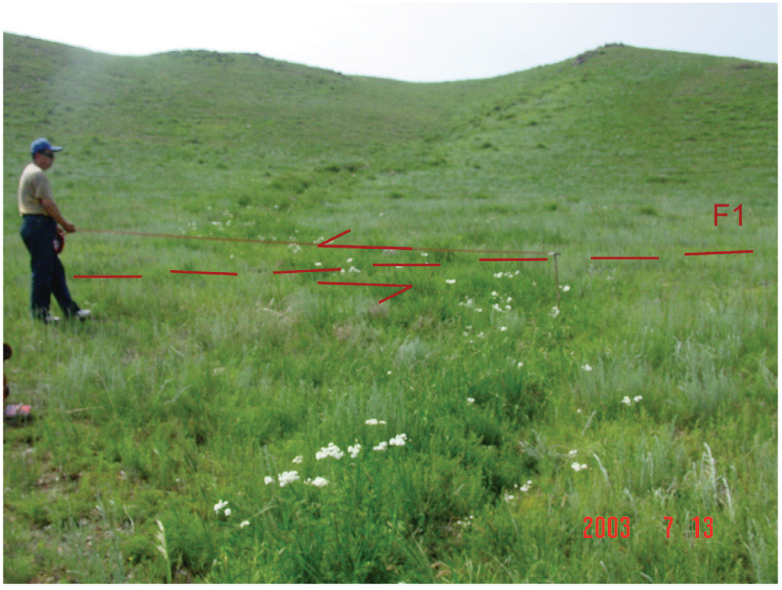

Fig. 4. Photo of stream offsets, camera to NE, showing active fault (F1) resulted in observed maximum displacement of a stream (5 m).

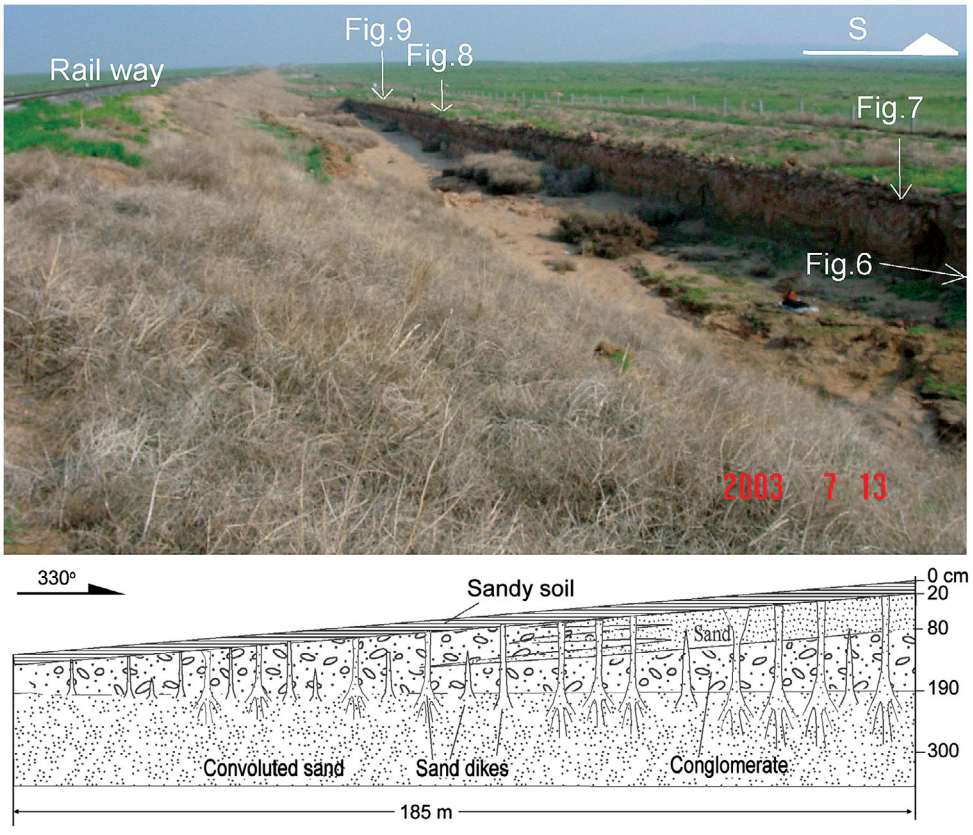

Fig. 5. Schematic diagram and photo at the site P1, showing paleo-ground ruptures, fissures, sand dikes and the sites of Figs. 6 to 9.

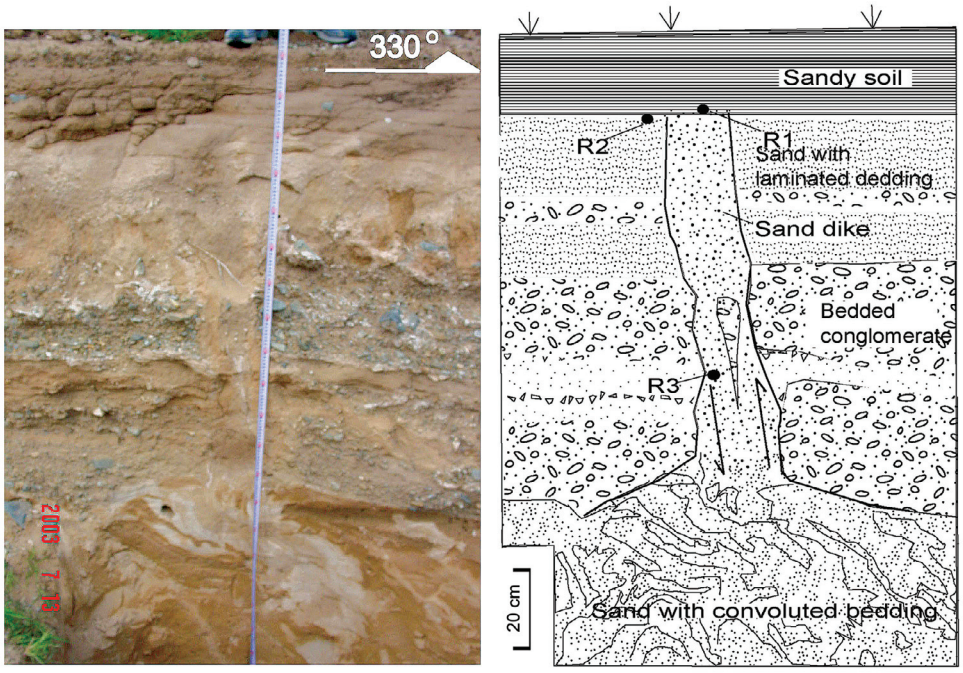

Fig. 6. Photo and corresponding charcoal drawing of a ground rupture of about 20-cm wide and 230-cm deep on P1, displaying sand dikes covered by thin soil, convoluted sands caused by liquefaction, and the sites of dating samples R1, R2 and R3.

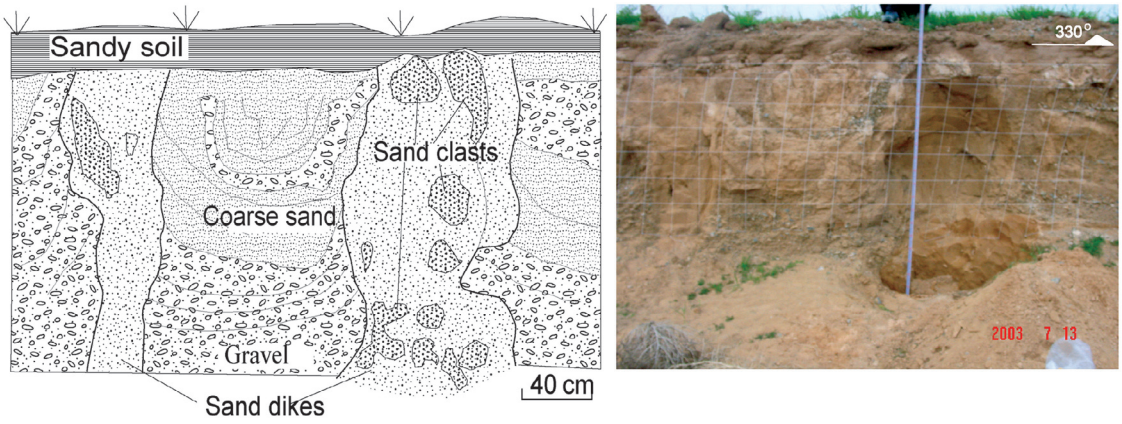

Fig. 7. Photo and drawing of a ground rupture, showing syncline in Later Pleistocene gravel layers and sand dikes. Grids in the photo are 20 × 20 cm.

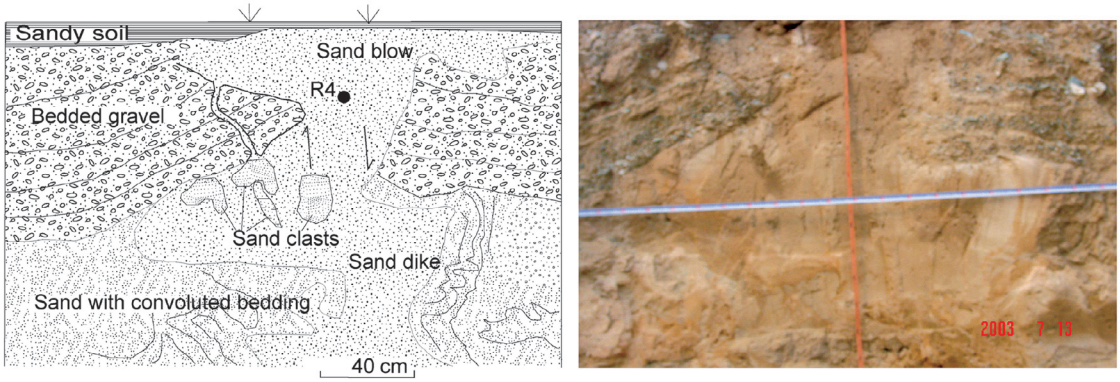

Fig. 8. Photo and drawing of a ground rupture, displaying displacement of bedded gravel and geometric features of sand dikes and sand blows. The gravel on the upper plate was uplifted from near level to a slope of about 30° by upward hydraulic force and horizontal compression.

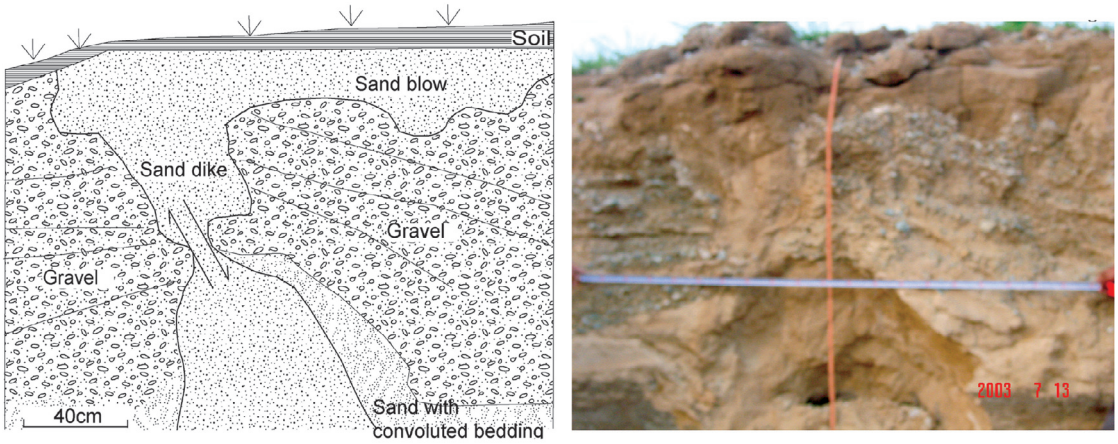

Fig. 9. Photo and drawing of a ground rupture, showing features of sand dike, broken gravel layers and liquefied sand, upward hydraulic force deformed gravel layers with small vertical displacements.

Table 1. Thermoluminescence ages of sand samples.

Sample No.	Sample site	Age (ka)
R50	Top of ruptured sand, P3	13.4 ± 1.1
R1	Bottom of soil layer, P1	15.2 ± 1.3
R2	Sand flow, P1	19.3 ± 1.7
R4	Sand dike, P1	19.1 ± 1.6
R3	Sand dike, P1	32.3 ± 2.7
R150	Clast in ground rupture, P4	52.6 ± 4.5

structure (Fig. 10), which was caused by upwards hydraulic flow that carried away small-grain sands, but the larger grains remained in the fissure. The larger grains are derived from the fluvial sediment as found at the SE part of this profile (Fig. 11). In the middle part of the profile, fluvial strata were severely disturbed, and there are some small intruded-sands consisting of sands and fine-grained gravels, indicating a hydraulic origin. In the SW section, disturbed structures in interlaminated coarse and fine-grained sands at a depth of 50 to 150 cm were found. A dike composed of fine-grained gravels and coarse sands was likewise found at a depth of 150 to 190 cm, with maximum width of 8 cm, and unconformably covered by a deformed thin gravel layer and 5-cm thick gravel fill at the top of the ground fissure (Fig. 11), indicating that this fissure was formed earlier than the fissure in the NW area of P3 (Fig. 10). In addition, the host sands of the deeper sand dike are older than those at the NW part of the profile. The fissures and sand dikes at different depths were formed by at least two events of ground shaking, indicating that seismic recurrence has occurred in the study area after the Late Pleistocene.

At the SE end of P4, a ground fissure of 11 cm wide at the top was found within a depth of 100 - 150 cm. A sand clast with grayish dark spots, 10 cm in diameter, exists in the fissure and has an age of 53 ka (Table 1). The 5-cm wide dike consists of medium-grained buff sand, which is adjacent to the left (SE) of the sand clast (Fig. 12). The clast has the same mineral composition of the top part of host sands. At the NW end of P4, two ground fissures are 1 m apart and covered with surface soil. The fissures are 50 to 80 cm wide and more than 70 cm deep. They are filled with medium to coarse yellow sands, clasts of host sediments consisting of siltic brown and gray blocks, and about 1-cm-thick fine-grained gray gravel distributed discontinuously at the bottom of the dikes (Fig. 13). The dikes may be seismically intruded because their structures are related to sand flow, which are different from those filled by human activity or other mechanisms. The materials could be derived from the liquefied fluvial sediments. The fissures and sand blows at different depths could have been caused by multiple past occurrences of ground shaking and hydraulic flows.

4. DISCUSSION

When estimating the strength of a paleoearthquake, one fundamental task is to identify whether the features are of seismic origins (Obermeier 1996). The effects of fluidization are first discussed in the following section. Two techniques for estimating the magnitude and intensity of paleoearthquakes are the magnitude bound method, which uses the most distal site of liquefaction from the energy center (Ambraseys 1988; Obermeier and Pond 1999), and the other uses the empirical relationship between earthquake

magnitude (M) and the length (L, in km) of the rupture zone in eastern China (Dong et al. 1993).

4.1 Origin of Liquefaction Features

Sand dikes, ground ruptures and fissures can be of seismic or aseismic origins. Aseismic causes, such as volcanic activity, glacial ice wedge, artesian pressures, aseismic landsliding, and preferential weathering cannot be attributed the aforementioned liquefaction features in the study area, as discussed below.

Volcanic activity associated with earthquakes can result in sand liquefaction. Volcanic activity can generate structures that give rise to vents or tubular conduits, and can cause injection of materials, fractures, infills, alterations, etc., as a consequence of the ejection of fluids, gases, and other materials (González de Vallejo et al. 2005). There are many volcanoes in the study area. The volcanoes are older

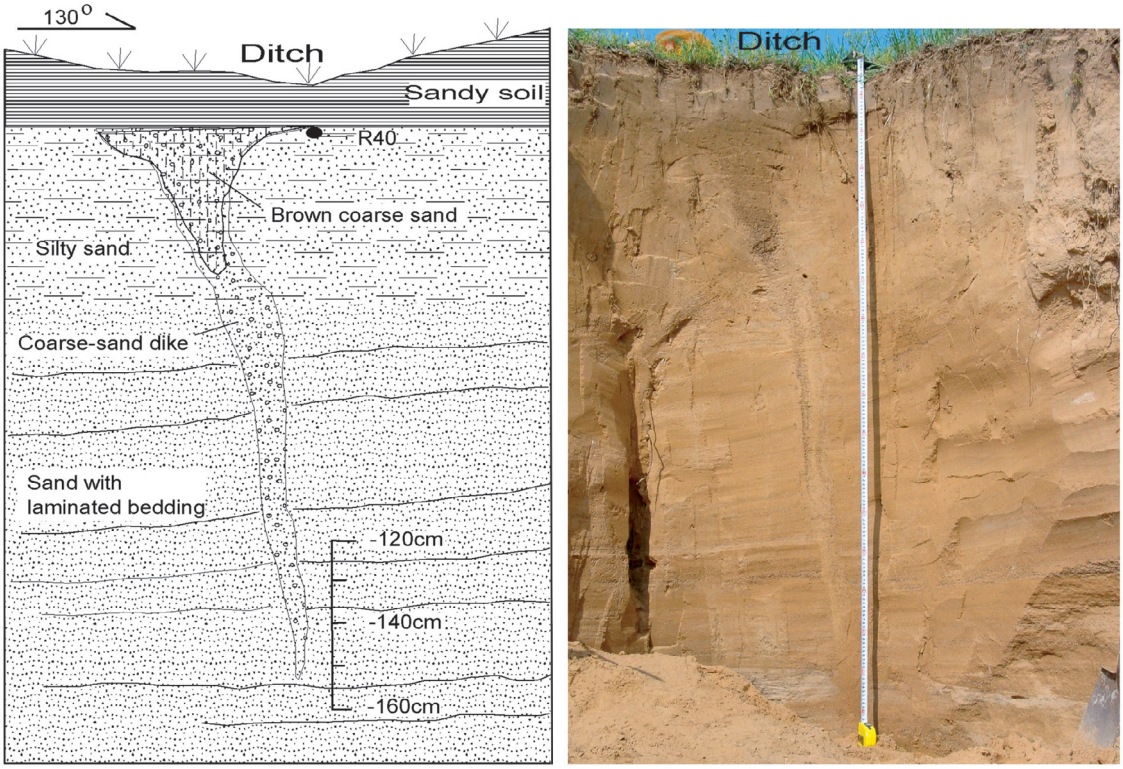

Fig. 10. Photo shows a ground fissure on which an approximately 15-cm deep ditch with a strike of NE formed; the charcoal drawing describes a ground fissure and the dating sample position (R50), location: 43°37'23.9"N, 115°39'38.8"E.

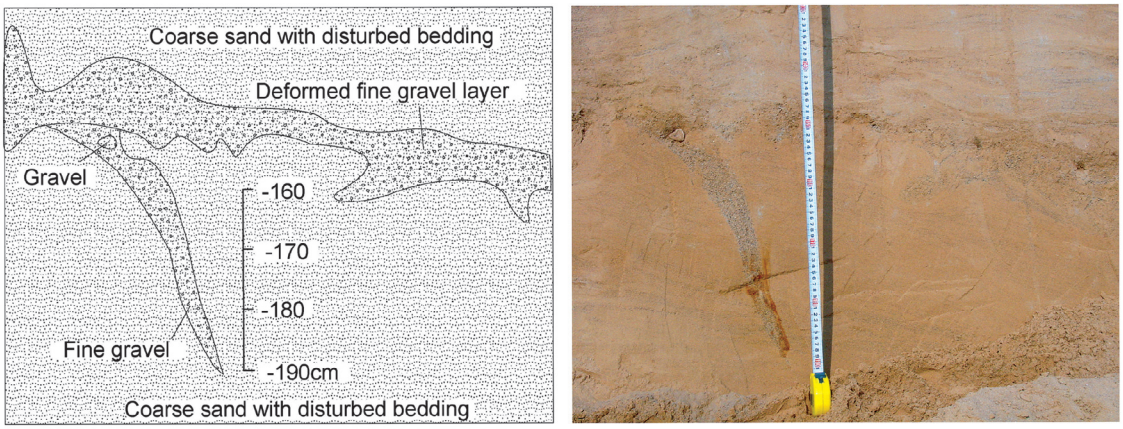

Fig. 11. Diagram of the ground fissure and deformed gravel layer on P3. The minus scale numbers denote the depths from the surface.

than the host strata of dikes and deformed layers, thus ruling out a direct relation between any volcanic activity and the observed liquefaction effects.

Ice wedge casts are characterized by downward-pinching, planar, nearly vertical features that originated by thermal contraction of frozen ground. Ice wedges grow wider during cold episodes. Conversely, host sediments slowly replace the melting ice when permafrost melts (Obermeier 1996). The latitude of the study area is from about 43 to 44°N, and elevation ranges from about 1000 to

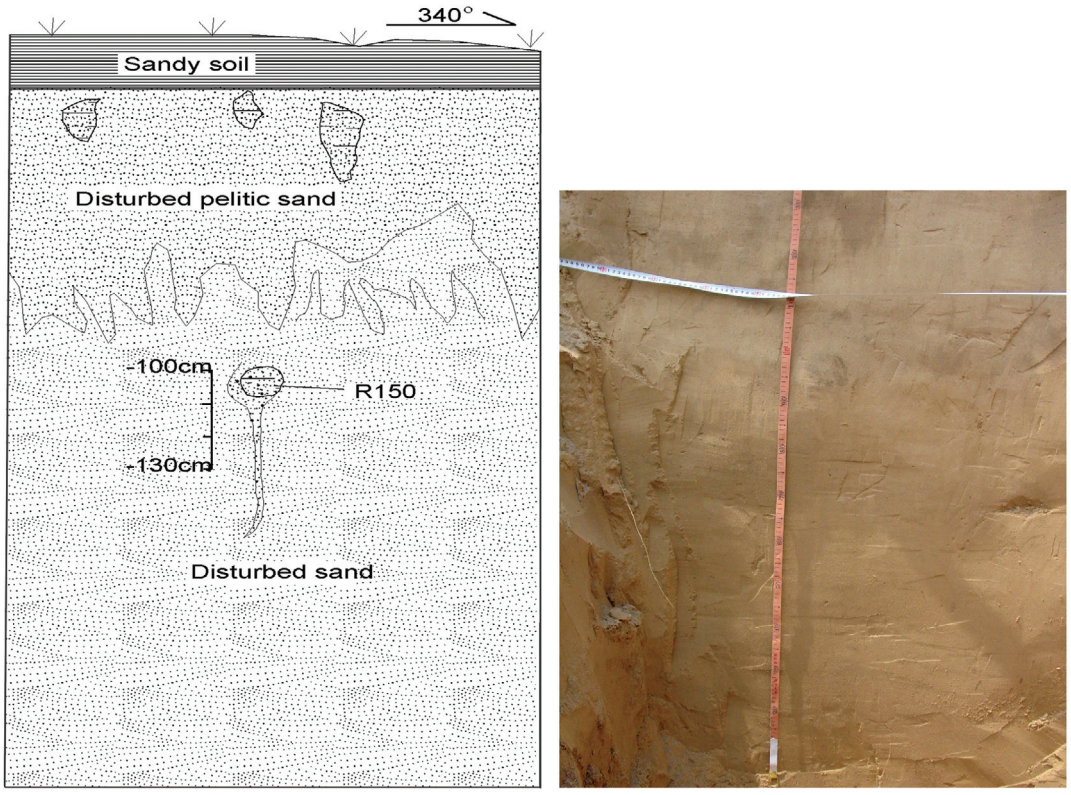

Fig. 12. Photo and drawing of the features of ground fissures and liquefaction at P4 in Fig. 2 (44°31'28.9"N and 117°41'14.8"E). Sand liquefaction resulted in paleo-surface fissures and the layer boundary is severely deformed at a depth of 60 - 80 cm. The sandy lump with grayish dark spots at a depth of 100 - 110 cm is 10 cm in diameter and 53 ka BP (R150). Note that the patterns in the Figs. 12 and 13 have no sediment structure meaning, just stand for what are marked and described in the text.

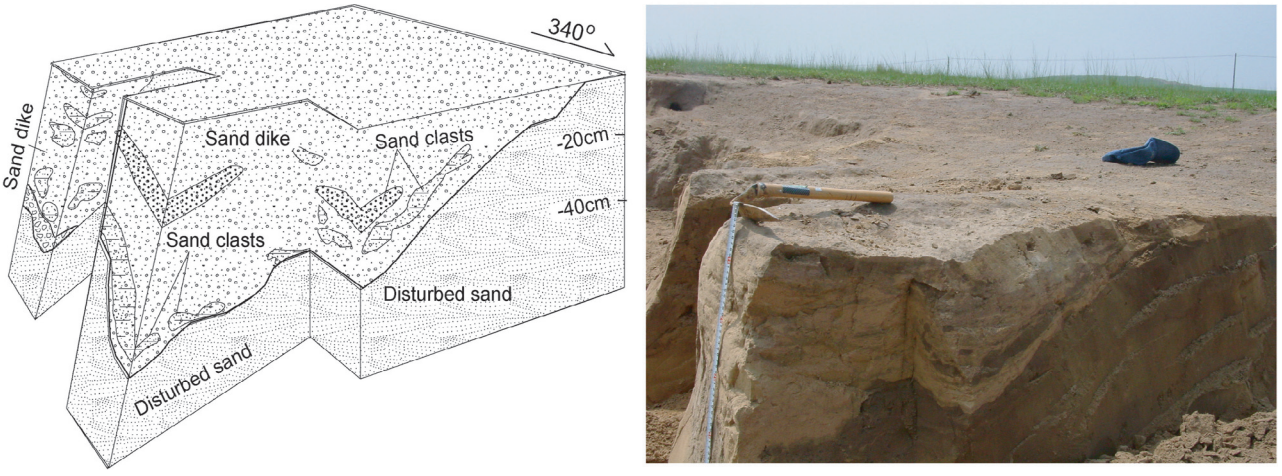

Fig. 13. Photo and corresponding drawing of two 70-cm width ground fissures filled with colorful sandy and pelitic lumps and buff sand, and gravel at the top of the disturbed sand at P4 in Fig. 2.

1300 m. The maximum thickness of the frozen ground layer in the shade is 120 cm during the winter (generally 80 cm in recent years), which is much shallower than most of the observed sand dikes. Neither glaciers nor glacial tills are found in the region. Currently, the liquefied sands are tens of meters above the water table in the study area where ground water is rarely exploited. The Xilinhot district has been tectonically uplifted since the middle of the Pleistocene, indicating the elevation was lower before the fissure formation and the climate was warmer. Additionally, at about 500 m northeast of P1, no fissures were found in another trench which contains the same Quaternary strata. Therefore, the liquefaction effects, such as the older age of dike sands, upward hydraulic flow and dike sands, and folds were unlikely to be caused by glaciers or ice wedges.

The study area is categorized as a highland and arid area. The deformed strata that host the sand dikes and paleo-ground ruptures/fissures are clastic alluvia. The liquefied sands, deposited originally in lacustrine and fluvial environments, widely occurred in the area and the gravel layer contains folds. The sands in the dikes are the same as the liquefied sands, excepting P1. Additionally, the surface tip angle is less than 15° in the sites except for P2, and no evidence of landslides were observed in the field. Thus it is implausible that landslides caused the observed features in the area.

Artesian pressure in confined aquifers may cause artesian sand flows. However, the important fact is that no aquifuge on the liquefied sands was observed, but coarse sands and gravels (Fig. 3), indicating the liquefied sands act as a phreatic aquifer. The hydraulic pressure of liquefied sands in the area should not be high because the relative differences in elevation are small in the plateau region where the climate is generally arid. Therefore, the observed features of liquefaction can not be attributed to artesian sand flows.

Consequently, the geological evidence shows that the dikes, paleo-ground ruptures and fissures are most likely resulted from ground shaking associated with seismic fault activity.

4.2 Age of Paleoseismic Events

Sand samples for dating were collected with opaque plastic cassettes for thermoluminescence dating because sedimentary organic materials for ^{14}C dating were unavailable. The ages of the samples were determined using thermoluminescence technique (Fattahi 2008) with a F427-A thermoluminescence dosimeter at the Institute of Crustal Dynamics, China Earthquake administration (Table 1).

The Holocene surface soil can be considered as a horizon marker that covers the surface ruptures and fissures directly. Fissures and sand blows in the observed sites may correspond to the last seismic event. Therefore, for estimating the upper and lower age bounds of the last seismic event, we determined the maximum age of the soil and the minimum age of the ruptured sand layer.

The age of sands at the soil bottom developed in the sand blow is 15.2 ± 1.3 ka (R1) in P1, which is attributed to mixture of older sand from the lower liquefied source sands. However, the top of the host sands (R50) was dated as 13.4 ± 1.1 ka old in P3. The upper part of sand dike has an age of 19.3 ± 1.7 ka (R2) and the lower parts of the sand dikes have ages of 19.1 ± 1.6 ka (R4) and 32.3 ± 2.7 ka (R3). Additionally, the age of the clast in an older rupture in P4 is 52.6 ± 4.5 ka (Table 1: R150). Samples (R3 and R4) of sand dikes are older because of a mixture of older sands from the liquefied source sands, as shown in Fig. 5, ruling out the possibility that surface sands or upper sands in the vertical section fell into the fissures. The paleo-surface that formed on the fissured strata is unconformable with the Holocene soil layer that was formed by erosion after the last paleoearthquake and can be considered as a key bed in the region (Fig. 3). Therefore, the maximum age of the last seismic event is possibly about 13 ka based on the dating results (Table 1) and assuming that these features were caused by either one earthquake or more earthquakes and rapidly covered by the Holocene soil.

The older age of the sand clast filled ground fissures (R150) and paleo-ground ruptures and fissures of different ages found in P3 and P4 (Figs. 10, 12) may indicate that multiple paleoearthquakes occurred in the area since the middle Pleistocene. Additional data will be needed to confirm the timing of paleoearthquakes.

4.3 Magnitude of Paleoearthquakes

Surface ruptures and fissures along active faults are considered one of the most important types of evidence for strong earthquakes. For example, the 1931 Fuyun M_s 8.0 earthquake, Xinjiang, northwestern China produced a rupture zone approximately 170 km long (XJUARBS 1985); The 8 November 1997 Manyi M_w 7.6 earthquake caused a 170 km-long rupture zone (Peltzer et al. 1999); as well as the 14 November 2001 Kunlun M_w 7.8 earthquake in the northern Tibet produced a 430 km-long surface rupture zone (Xu et al. 2002; Fu et al. 2005). The epicenter location and the magnitude of the earthquake are related to geometric parameters of surface ruptures (Deng et al. 1992; Wells and Coppersmith 1994; McCalpin 1996; Ran and Deng 1999). A number of upper bounds for earthquake magnitude that describe the relationship between earthquake magnitude (M_s) and epicentral (R_e) and fault (R_f) distances of liquefaction have been proposed (Ambraseys 1988; Papathanassiou et al. 2005). As mentioned before, the geological and geographic evidence along fault F1 suggests that two possible scenarios to explain these paleoseismic features: the observed paleo-ground ruptures/fissures, sand blows, and sand dikes were caused by one seismic event. Assuming that the hydrologi-

cal and sedimentary conditions were similar at the observed sites, the values of peak ground acceleration decrease with increasing epicentral distance, so the other scenario to explain our observations is that resulted from multiple seismic events having magnitudes greater than 6.0.

In the first case, the magnitude of this paleoearthquake is estimated to be M_s 6.6 to M_s 7.5 based on an assumed rupture zone length of 150 to 200 km and the relationship $M = 4.09 + 1.699 \times 10^{-2} L$ between large earthquake magnitude (M_s) and length (L in km) of rupture zone in eastern China (Dong et al. 1993). Otherwise, using a epicentral distance (R_e) of 150 km, the paleoearthquake magnitude is estimated at M_s 6.7 according to $M_s = 4.742 + 4.655 \times 10^{-3} R_{emax} + 0.8907 \log(R_{emax})$(Papathanassiou et al. 2005). Using the formula from $\log(R_e) = 0.77(M) - 3.60$ (Ambraseys 1988), the estimated magnitude would be M 7.5. Therefore, considering the uncertainty, these results suggest that the maximum magnitude between 6.6 and 7.5 for the most recent earthquake which likely occurred at about 13 ka BP along faults F1 or F2.

The width of surface rupture zone is more than 200 m at P1 and becomes narrower and narrower with increasing distance from P1. In addition, the widths of ground ruptures/dikes become smaller away from P1. These may indicate that the values of ground peak acceleration decreased away from P1 (assuming that sediment conditions at the sites were similar). Similarly, Audemard et al. (2005) reported that the 23 June 2001 Arequipa M_w 8.4 earthquake on the southern coast of Peru caused highly asymmetrical distributions of liquefaction features, with the width of isolated sand blows decreased with increasing epicentral distance. An excellent example of using dike widths to approximate the location of the meizoseismal region was given by Munson et al. (1995). Therefore, we infer that there may be the possibility that site P1 is located in the meizoseismal area for the most recent large paleoearthquake based on the limited observations available thus far.

In the second case, resulting from multiple seismic events with magnitudes ≥ 6.0, is also reasonable because ground rupture and sand liquefaction in northern China has usually resulted from earthquakes with magnitudes ≥ 6.8 (Deng et al. 1992; Dong et al. 1993). The fissures and liquefaction features in P3 and P4 illustrate the reoccurrence of large earthquakes since the Middle Pleistocene. Two earthquakes with M_s 5.7 and 5.9 occurred within the vicinity study area in 2003 and 2004 (Fig. 1) did not result in any ground ruptures, large fissures and liquefactions in the valleys.

Bonilla (1988) suggested that the threshold magnitude for triggering surface faulting is around 6. The epicentral areas for the strong paleoearthquakes may be near the different segments of the active faults (F1 and F2 in Fig. 2), and possibly at least one of the meizoseismal areas is located near P1. The number and scale of fissures and rupture are large in meizoseismal areas, which agrees with the results of Obermeier and Pond (1999), interpreting dikes spreading laterally and extending more than a kilometer at many places in the meizoseismal zone of the 1811 - 1812 New Madrid earthquakes in Missouri.

4.4 Seismic Intensity

Paleoearthquake magnitudes and the sizes of active faults and ruptures are important parameters for estimating the intensity of paleoearthquakes. The observed ruptures and fissures, combined with the remote image, suggest that seismic intensity was at least VIII (MM) in the meizoseismal area, as discussed below. An intensity of about VI is the threshold for widespread development of small-scale soft-sediment deformation features (Obermeier 1996). The minimum intensity for inducing liquefaction features is commonly considered VII, and values of VIII and IX were generally required before liquefaction-induced ground failure become severe enough to cause damage to buildings (McCalpin 1996; Obermeier 1996). The length of the active fault (Fig. 2) and estimated magnitude of the last large prehistoric earthquake indicate that the epicentral intensity in the studied area would likely be at least VIII (MM). This is also supported by the fact that the intensity of the 16 August 2003 M_s 5.9 earthquake which occurred in the study area (Fig. 1) was VIII (MM) in the epicentral area of about 170 km^2 (Gao et al. 2005). Moreover, using a paleoearthquake magnitude range from 6.6 to 7.5, the epicentral intensity is estimated to be from about X to less than XII (MM) using the simple equation of epicentral intensity (I_o) and surface wave magnitude ($M_s = 1.06 + 0.56 I_o \pm 0.37$, Romeo and Pugliese 2000). Therefore, the intensity in the paleomeizoseismal area could reasonably have been larger than IX (MM), and seismic intensity in a majority of the Xilinhot district likely would be higher than VI (MM).

5. CONCLUSIONS

Geological and geographic evidences in the Xilinhot region demonstrate that there is a huge surface rupture and fissure zone with a maximum length from 150 to 200 km and a width of larger than 200 m along fault F1 related to paleoearthquakes. The huge surface rupture zone and dating data indicate that a large paleoearthquake likely with a maximum magnitude from 6.6 to 7.5, or multiple seismic events with M ≥ 6.0 possibly occurred at about 13 ka BP, and that strong earthquakes and fault activities likely repeatedly occurred after the Middle Pleistocene. The new findings of active faults, paleoseismic liquefaction features and seismic activity of $M_s > 5$ in recent years in the Xilinhot district and vicinity demonstrate that seismic activity and intensity have been underestimated in the region. The epicentral intensity from a repeat of one of the paleoearthquakes likely would

be at least IX (MM), and seismic intensity would be larger than VI in the study area, but seismic intensity in the region has been estimated to be less than VI (CSB 1991). Thus, the engineering constructions should be designed to resist future potentially large earthquakes. Further investigations of segmentation and displacement of faults and additional knowledge regarding the recurrence and intensity of earthquakes in the Xilinhot district will be needed to better understand seismicity in this region.

Acknowledgements The authors are grateful to Dr. M. Leckner (Concordia University) grammatically improving the manuscript, and thank Prof. K. Takemura in Kyoto University and Dr. Ronald Green in Inst. Eng. for their constructive comments. We also wish to express our thanks to Prof. Yu-Chang Chan and another anonymous reviewer for their comments and the colleagues in Xilinhot Bureau of Seismology for great help during the field investigations. This work was supported by Ministry of Science and Technology (No. 2005DFA20980), the Earthquake Science Foundation, China (No. B07002) and Kyoto University.

REFERENCES

Ambraseys, N. N., 1988: Engineering seismology: Part I. *Earthq. Eng. Struct. Dyn.*, **17**, 1-50, doi: 10.1002/eqe.4290170101. [Link]

Audemard, M. F. A., J. C. Gómez, H. J. Tavera, and G. N. Orihuela, 2005: Soil liquefaction during the Arequipa M_w 8.4, June 23, 2001 earthquake, southern coastal Peru. *Eng. Geol.*, **78**, 237-255, doi: 10.1016/jenggeo.2004.12.007. [Link]

BGMRIM (Bureau of Geology and Mineral Resources of Inner Mongolia Autonomous Region), 1991: Regional Geology of Inner Mongolia Autonomous Region, Geological Publish House, Beijing, 598 pp. (in Chinese)

Bonilla, M. G., 1988: Minimum earthquake magnitude associated with coseismic surface faulting. *Bull. Assoc. Eng. Geol.*, **25**, 17-29.

CSB (China Seismological Bureau), 1991: Regionalization Map of Earthquake Intensity in China (The third version), Seismological Press, Beijing, 1 p. (in Chinese)

CSB (China Seismological Bureau), 2001: The Zoning map of Ground Vibration Parameters in China (GB 18306-2001) (the fourth version), Seismological Press, Beijing, 1 p. (in Chinese)

Deng, Q., G. Yu, and W. Ye, 1992: Relationship between earthquake magnitude and parameters of ground rupture. In: SAF Editorial Boarder (Eds.), Study on Active Fault (2), Seismological Press, Beijing, 247-264. (in Chinese)

Ding, G., 1991: Introduction of Lithosphere Dynamics in China - Description of Atlas of Lithosphere Dynamics in China, Seismological Press, Beijing, 289-294. (in Chinese)

Dong, R., H. Ran, and Z. Gao, 1993: The relationship between earthquake magnitude and length of active fault in China. *Seismol. Geol.*, **15**, 395-400. (in Chinese)

Fattahi, M., 2008: Dating past earthquakes and related sediments by thermoluminescence methods: A review. *Quat. Int.*, **199**, 104-146, doi: 10.1016/j.quaint.2008.06.015. [Link]

Fu, B., A. Lin, K. I. Kano, T. Maruyama, and J. Guo, 2003: Application of stereoscopic satellite images for studying Quaternary tectonics in arid regions. *Int. J. Remote Sens.*, **25**, 537-547, doi: 10.1080/01431160310000150031. [Link]

Fu, B., Y. Ninomiya, X. Lei, S. Toda, and Y. Awata, 2004: Mapping active fault associated with the 2003 M_w 6.6 Bam (SE Iran) earthquake with ASTER 3D images. *Remote Sens. Environ.*, **92**, 153-157, doi: 10.1016/j.rse.2004.05.019. [Link]

Fu, B., Y. Awata, J. Du, Y. Ninomiya, and W. He, 2005: Complex geometry and segmentation of the surface rupture associated with the 14 November 2001 great Kunlun earthquake, northern Tibet, China. *Tectonophysics*, **407**, 43-63, doi: 10.1016/j.tecto.2005.07.002. [Link]

Gao, M., L. Xu, W. Guo, B. Wan, and Y. Yu, 2005: Spatial damage distribution of Augst 16, 2003, Inner Mongolia, China, M_s = 5.9 earthquake and analysis. *Acta Seismol. Sin.*, **18**, 218-225, doi: 10.1007/s11589-005-0069-x. [Link]

González de Vallejo, L. I., M. Tsigé, and L. Cabrera, 2005: Paleoliquefaction features on Tenerife (Canary Islands) in Holocene sand deposits. *Eng. Geol.*, **76**, 179-190, doi: 10.1016/j.enggeo.2004.07.006. [Link]

Green, R. A., 2001: Energy-based evaluation and remediation of liquefiable soils. Ph.D Thesis, Civil Engineering Dept., Virginia Tech, Blacksburg, VA. 397 pp.

Green, R. A., S. F. Obermeier, and S. M. Olson, 2005: Engineering geologic and geotechnical analysis of paleoseismic shaking using liquefaction effects: Field examples. *Eng. Geol.*, **76**, 263-293, doi: 10.1016/j.enggeo.2004.07.026. [Link]

Huang, C., Y. C. Chan, J. C. Hu, J. Angelier, and J. C. Lee, 2008: Detailed surface co-seismic displacement of the 1999 Chi-Chi earthquake in western Taiwan and implication of fault geometry in the shallow subsurface. *J. Struct. Geol.*, **30**, 1167-1176, doi: 10.1016/j.jsg.2008.06.001. [Link]

McCalpin, J. P., 1996: Paleoseismology, Academic Press, Inc., San Diego, 588 pp.

Munson, J., C. A. Munson, and E. C. Pond, 1995: Paleoliquefaction evidence for a strong Holocene earthquake in south-central Indiana. *Geology*, **23**, 325-328, doi: 10.1130/0091-7613(1995)023<0325:PEFASH>2.3.CO;2. [Link]

Obermeier, S. F., 1996: Use of liquefaction-induced features for paleoseismic analysis - An overview of how seismic liquefaction features can be distinguished from other features and how their regional distribution and properties of source sediment can be used to infer the location and strength of Holocene paleo-earthquakes. *Eng. Geol.*, **44**, 1-76, doi: 10.1016/S0013-7952(96)00040-3. [Link]

Obermeier, S. F., 1998: Liquefaction evidence for strong earthquakes of Holocene and latest Pleistocene ages in the states of Indiana and Illinois, USA. *Eng. Geol.*, **50**, 227-254, doi: 10.1016/S0013-7952(98)00032-5. [Link]

Obermeier, S. F. and E. C. Pond, 1999: Issues in using liquefaction features for paleoseismic analysis. *Seismol. Res. Lett.*, **70**, 34-58.

Olson, S. M., R. A. Green, and S. F. Obermeier, 2005: Geotechnical analysis of paleoseismic shaking using liquefaction features: A major updating. *Eng. Geol.*, **76**, 235-261, doi: 10.1016/j.enggeo.2004.07.008. [Link]

Papathanassiou, G., S. Pavlides, B. Christaras, and K. Pitilakis, 2005: Liquefaction case histories and empirical relations of earthquake magnitude versus distance from the broader Aegean region. *J. Geodyn.*, **40**, 257-278, doi: 10.1016/j.jog.2005.07.007. [Link]

Peltzer, G., F. Crampé, and G. King, 1999: Evidence of nonlinear elasticity of the crust from the M_w 7.6 Manyi (Tibet) earthquake. *Science*, **286**, 272-276, doi: 10.1126/science.286.5438.272. [Link]

Prestininzi, A. and R. Romeo, 2000: Earthquake-induced ground failures in Italy. *Eng. Geol.*, **58**, 387-397, doi: 10.1016/S0013-7952(00)00044-2. [Link]

Ran, Y. and Q. Deng, 1999: History, actuality and future of paleoseismology. *Chin. Sci. Bull.*, **44**, 12-20.

Romeo, R. and A. Pugliese, 2000: Seismicity, seismotectonics and seismic hazard of Italy. *Eng. Geol.*, **55**, 241-266, doi: 10.1016/S0013-7952(99)00081-2. [Link]

Tuttle, M. P., 2001: The use of liquefaction features in paleoseismology: Lessons learned in the New Madrid seismic zone, central United States. *J. Seismol.*, **5**, 361-380, doi: 10.1023/A:1011423525258. [Link]

Vanneste, K., K. Verbeeck, T. Camelbeeck, E. Paulissen, M. Meghrouui, F. Renardy, D. Jongmans, and M. Frechen, 2001: Surface-rupturing history of the Bree fault scarp, Roer Valley graben: Evidence for six events since the late Pleistocene. *J. Seismol.*, **5**, 329-359, doi: 10.1023/A:1011419408419. [Link]

Wells, D. L. and K. J. Coppersmith, 1994: New empirical relationships among magnitude, rupture length, rupture width, rupture area, and surface displacement. *Bull. Seismol. Soc. Am.*, **84**, 974-1002.

XJUARBS (Xinjiang Uygur Autonomous Region Bureau of Seismology), 1985: Fuyun Earthquake Fault Zone, Seismological Press, Beijing, 206 pp. (in Chinese)

Xu, X., W. Chen, G. Yu, W. Ma, H. Dai, Z. Zhang, Y. Chen, W. He, Z. Wang, and G. Dang, 2002: Characteristics of the surface ruptures of the Hohsaihu (Kunlunshan) earthquake (M_s 8.1), Northern Tibetan plateau, China. *Seismol. Geol.*, **24**, 1-17. (In Chinese)

Yeats, R. S., K. Seih, and C. R. Allen, 1997: The Geology of Earthquakes, Oxford University Press, New York, 568 pp.